Magnetic silhouettes in Jupiter's non-auroral ionosphere

Article

Published Version

Knowles, K. L., Stallard, T. S., O'Donoghue, J. ORCID: https://orcid.org/0000-0002-4218-1191, Moore, L., Agiwal, O., Melin, H., Roberts, K., Tiranti, P. I., Rae, I. J., Thomas, E. M., Connerney, J. E. P. and James, M. K. (2025) Magnetic silhouettes in Jupiter's non-auroral ionosphere. Journal of Geophysical Research: Space Physics, 130 (5). e2025JA033868. ISSN 2169-9402 doi: 10.1029/2025JA033868 Available at https://centaur.reading.ac.uk/122837/

To link to this article DOI: http://dx.doi.org/10.1029/2025JA033868

Publisher: American Geophysical Union

ADVANCING EARTH AND SPACE SCIENCES

JGR Space Physics

RESEARCH ARTICLE
10.1029/2025JA033868

Magnetic Silhouettes in Jupiter's Non-Auroral Ionosphere

K. L. Knowles[1], T. S. Stallard[1], J. O'Donoghue[2], L. Moore[3,4], O. Agiwal[3,4], H. Melin[1], K. Roberts[4], P. I. Tiranti[1], I. J. Rae[1], E. M. Thomas[1], J. E. P. Connerney[5,6], and M. K. James[7]

[1]Department of Mathematics, Physics and Electrical Engineering, Northumbria University, Newcastle-upon-Tyne, UK, [2]Department of Meteorology, University of Reading, Reading, UK, [3]Department of Astronomy, Boston University, Boston, MA, USA, [4]Center for Space Physics, Boston University, Boston, MA, USA, [5]Space Research Corporation, Annapolis, MD, USA, [6]NASA Goddard Space Flight Center, Greenbelt, MD, USA, [7]School of Physics and Astronomy, University of Leicester, Leicester, UK

Key Points:

- Jupiter's ionospheric emissions are found to strongly correlate with the geometry of the magnetic field and are uniquely affected in each magnetic hemisphere
- The south exhibits a bimodality with the field's geometry, whereas the north shows a multi-modal relationship, with field strength providing an additional effect
- Ionospheric variations may be driven by energetic particle precipitation from the inner magnetosphere, and/or vertical ion drifts within the upper atmosphere

Supporting Information:

Supporting Information may be found in the online version of this article.

Correspondence to:

K. L. Knowles,
k.knowles@northumbria.ac.uk

Citation:

Knowles, K. L., Stallard, T. S., O'Donoghue, J., Moore, L., Agiwal, O., Melin, H., et al. (2025). Magnetic silhouettes in Jupiter's non-auroral ionosphere. *Journal of Geophysical Research: Space Physics*, *130*, e2025JA033868. https://doi.org/10.1029/2025JA033868

Received 20 FEB 2025
Accepted 1 MAY 2025

Author Contributions:

Conceptualization: T. S. Stallard
Formal analysis: K. L. Knowles, O. Agiwal
Investigation: K. L. Knowles
Methodology: T. S. Stallard
Software: M. K. James
Supervision: T. S. Stallard, I. J. Rae
Writing – original draft: K. L. Knowles
Writing – review & editing: K. L. Knowles, T. S. Stallard, J. O'Donoghue, L. Moore, O. Agiwal, H. Melin, K. Roberts, P. I. Tiranti, I. J. Rae, E. M. Thomas, J. E. P. Connerney

Abstract For decades, the influence of Jupiter's higher order magnetic field on its non-auroral ionosphere has remained enigmatic. NASA's Juno spacecraft has revealed great complexities in the Jovian magnetic field, with significant features in the sub-auroral regions aligning with puzzling structures identified in near-infrared emissions from the ionosphere. Here, we directly compare ground-based measurements of Jupiter's ionosphere with the latest magnetic field models borne in the era of Juno and reveal aspects of global ionosphere-magnetosphere coupling not previously explored. Ionospheric emissions exhibit either enhancements or reductions where the surface field is weakest and are found to correlate with both the strength and geometry of the magnetic field, where the latter is more dominant and with a unique control in each magnetic hemisphere. Therefore, we have illustrated that there may be distinct electrodynamic processes responsible for shaping Jupiter's non-auroral ionosphere in these key regions.

1. Introduction

Giant planet upper atmospheres are composed of a co-located neutral thermosphere, primarily consisting of molecular H_2 hydrogen, and a weakly ionized ionosphere, containing the collisionally-excited and prevalent molecular ion H_3^+. The near-infrared (NIR) emissions from H_3^+ are driven by its thermal excitation, and the observed intensity is governed by both the local ion density and the thermospheric temperature (Miller et al., 2013). Since planetary ionospheres mediate particle, energy and momentum transfer between the magnetosphere above and the turbulent atmosphere below, H_3^+ emissions and spectral measurements provide a unique window into their coupling at the Giant Planets. This allows us to remotely disentangle the physical properties of their tenuous upper atmospheres (Drossart et al., 1989; Geballe et al., 1993; Trafton et al., 1993), as well as providing a measure of particle precipitation and energy deposition into the system (Connerney & Satoh, 2000).

H_3^+ is formed from the ambient H_2 population, either by dayside solar photoionization from solar extreme ultraviolet radiation, or through particle impact ionization, often via electron precipitation about the magnetic poles (Miller et al., 2020). It is typically destroyed by dissociative recombination with free electrons, or through collisional proton exchange with "heavy" neutral species (Miller et al., 2020). While there are detailed ionospheric measurements within the auroral regions (Lam et al., 1997; T. Stallard et al., 2002; T. S. Stallard et al., 2018; Johnson et al., 2018), Jupiter's lower latitudes have remained relatively unexplored, and the extent of the coupling to the magnetosphere and atmosphere lacks observational constraints.

Equatorial NIR emissions are significantly fainter than the aurora and are difficult to spectrally separate from bright neutral species (Miller et al., 2020; T. S. Stallard et al., 2018). If the timescales of any transport processes are longer than the predicted chemical lifetime of H_3^+ (Miller et al., 2020; L. Moore et al., 2018), and since the incident solar flux is uniform across the planetary disk, emissions were thought to be relatively homogeneous, with a gradual gradient from the bright aurora down to the equator (Rego et al., 2000; T. S. Stallard et al., 2012). Unprecedentedly, recent works have instead revealed that the lower latitudes possess planet-wide variations in the ionospheric H_3^+ emissions (Drossart, 2019; Melin et al., 2024; O'Donoghue et al., 2021; T. S. Stallard et al., 2017; T. S. Stallard et al., 2018).

Analysis of long-term observations using the NASA Infrared Telescope Facility, utilizing H_3^+ filtered images averaged over 48 nights across 1995–2000, resulted in a map of the mean NIR emissions from Jupiter's

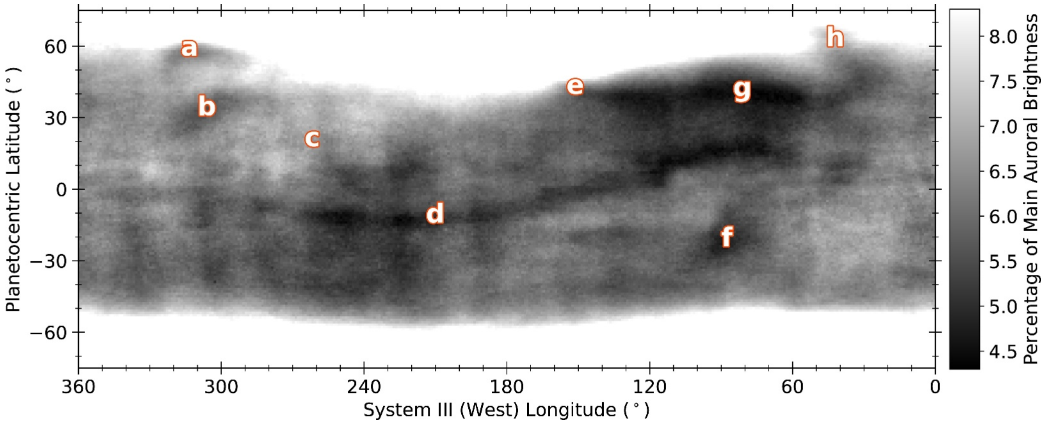

Figure 1. Mean infrared brightness of Jupiter's ionosphere, relative to the main auroral emission, with regions of brightening and darkening labeled a through to h. Only planetocentric latitudes up to 75° in magnitude, across all System III (West) longitudes, are displayed to represent the non-auroral ionosphere.

ionosphere (T. S. Stallard et al., 2018). This map, as shown in Figure 1, contains large-scale features with complex morphologies at weak brightness compared to the main auroral emission. In a given location, H_3^+ emissions may be depleted due to the region being cooler relative to its surroundings, a reduction in the local ion density, or both in tandem. Despite many features being later confirmed (Drossart, 2019), their driver has not been fully resolved, and they are not discernible in all measurements due to the sensitivity required to detect them (Lam et al., 1997; Melin et al., 2024; O'Donoghue et al., 2021).

Features of interest (The outlined latitudinal/longitudinal extents of the features represent approximate extents as seen in Figure 1 with the selected scaling, and do not represent the true physical boundaries of the emission features).

1. *The Great Cold Spot*. Previously identified as a region of 150 K cooling, approximately fixed in its magnetic position for a minimum of 15 years (T. S. Stallard et al., 2017), ranging across ∼280–320° System III (West) longitude and 45–62° North.
2. *Northern Ionospheric Anomaly*. Almost longitudinally co-aligned with the Great Cold Spot across ∼270–320°W, but further equatorward at 25–40°N, and larger.
3. *Broad region of enhancement*. Spanning across 290–320°W and 50–65°N.
4. *Dark Ribbon*. A sinusoidal ribbon of depleted H_3^+ emission, offset from the jovigraphic equator (within 20° either side), extending across all longitudes. Shown to be co-located with Jupiter's magnetic equator (T. S. Stallard et al., 2018), where field lines run parallel to the planet such that the dip angle, the angle between the magnetic field line and the local surface, is 0°.
5. *Head of the Northern Silhouette*. It "heads" into the northern aurora at 165°W and ∼40°N.
6. *Southern Ionospheric Dark Spot*. An isolated dark spot in the southern hemisphere, centered on 90°W and ∼25°S.
7. *Northern Silhouette*. At the largest scales, this is the darkest of all of the features, extending across ∼50–140°W in the northern hemisphere (30–45°N).
8. *Tail of the Northern Silhouette*. It "tails" the Northern Silhouette, and extends over 20–50°W and 30–70°N.

NASA's Juno mission has been taking extensive in-situ measurements of the Jovian magnetic field, resulting in higher-order planetary field and current sheet models in the era of Juno (Bloxham et al., 2022; Connerney et al., 2018; Connerney et al., 2020, 2022; K. M. Moore et al., 2017, 2019). Significant hemispheric asymmetries are persistent across recent models (Bloxham et al., 2022; Connerney et al., 2018; Connerney et al., 2022; Gastine et al., 2014; K. M. Moore et al., 2019) and include localized magnetic features away from the polar regions, such as a band of positive radial flux, "The Northern Hemispheric Flux Band," and an isolated area of intense, negative radial field in the south, "The Great Blue Spot" (Connerney et al., 2018). Following the completion of its prime mission in July 2021, the latest representation of the internal field is the JRM33 model (Connerney et al., 2022). Comparisons between JRM33 and its predecessor JRM09 (Connerney et al., 2018) identified a change over time

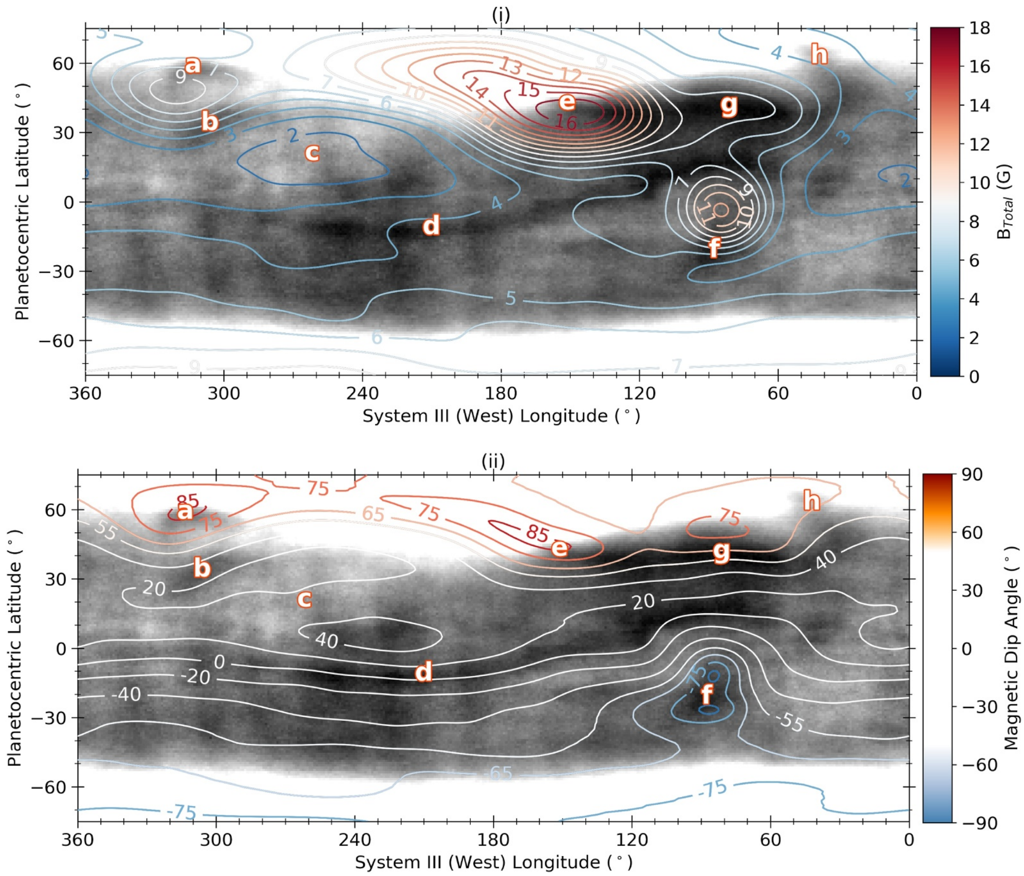

Figure 2. Contours of (i) total magnetic field strength (G) and (ii) magnetic dip angle (∘), projected onto the map of ionospheric emissions. For (ii), white contours indicate where the magnitude of the magnetic dip angle is below 50°, and red and blue depict where the dip angle is between positive and negative 55–90°, respectively.

on the sides of the Great Blue Spot due to its field being transported eastwards via shearing from vertically extended zonal winds (K. M. Moore et al., 2017, 2019).

This revelation of Jupiter's complex ionosphere (Drossart, 2019; Melin et al., 2024; O'Donoghue et al., 2021; T. S. Stallard et al., 2017, 2018), and the complementary discovery of its variable field (Connerney et al., 2022; K. M. Moore et al., 2017, 2019), make it compelling to compare the two unique data sets, and hints that Jupiter's powerful magnetic field may be responsible for the equatorial structure of its ionosphere. Here, we re-investigate observations originally presented in T. S. Stallard et al. (2018) and analyze the features of interest highlighted in Section 1. We discuss their possible connections with Jupiter's magnetic structure at non-auroral latitudes and draw our final conclusions in Section 2.

We utilize community code JupiterMag (James et al., 2022; Wilson et al., 2023) to use JRM33 and Con2020 (Connerney et al., 2020) as internal and external field models respectively. We assume a spherical planet with an equatorial radius of 71,492 km ($1R_J$) with the ionosphere ~550 km above the 1-bar pressure level (Melin et al., 2005). JRM33 assumes planetocentric System III East coordinates, but all mappings are transformed to planetocentric System III West. The incorporation of Con2020 is not significant at sub-auroral latitudes, where the radial component dominates, however we have utilized it for completeness.

2. Results and Discussions

2.1. The Strength and Geometry of the Jovian Magnetic Field

For Figure 2, we start by comparing the T. S. Stallard et al. (2018) observations of H_3^+ emissions from Jupiter's ionosphere with contours of (a) total magnetic field strength, B_{Total}, in Gauss and (b) magnetic dip angle in degrees,

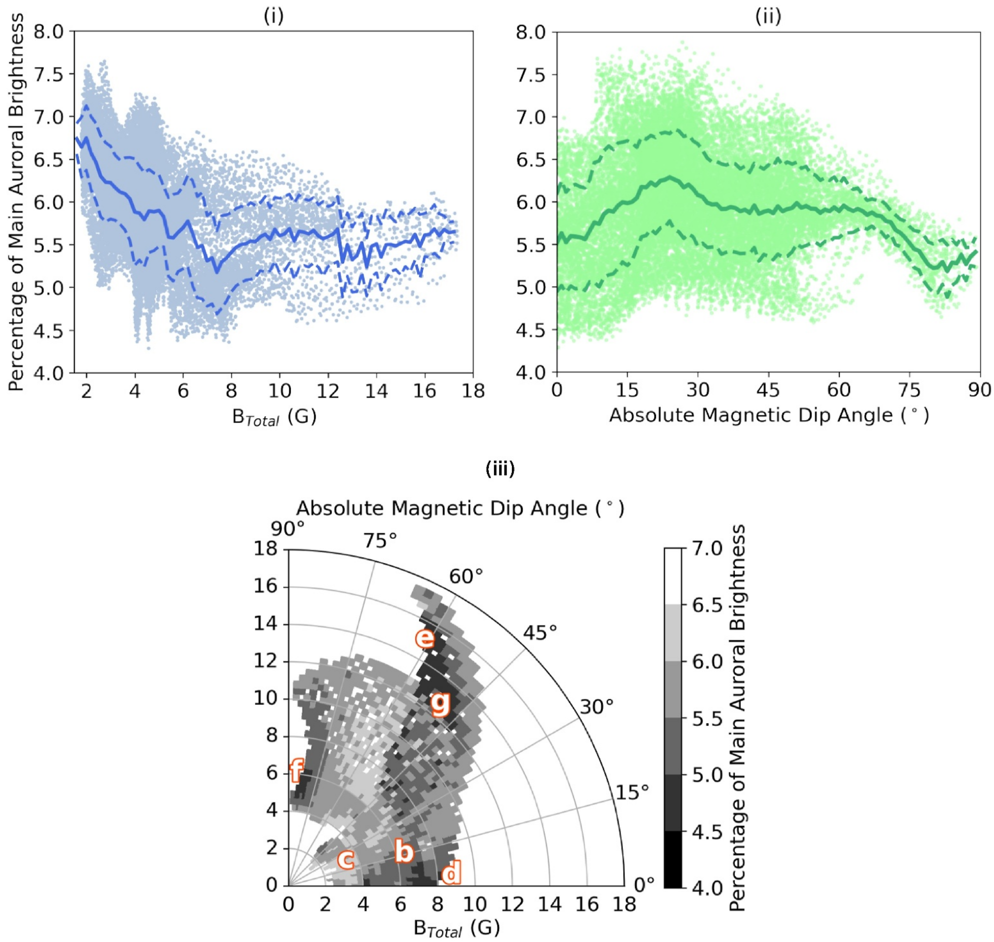

Figure 3. The relationship between the relative brightness of H_3^+ emissions and the (i) total magnetic field strength (G), (ii) magnetic dip angle (∘), as well as (iii) both parameters simultaneously between absolute latitudes of 35°. For (i, ii), the mean and standard deviations are shown in the solid and dashed lines, respectively. The area between 160 and 270°W and 25–35°N is masked due to the bright emissions from the aurora bleeding into the data.

where the latter represents the angle between the magnetic field line and the local horizontal surface (Rishbeth & Garriott, 1969). We display each of the components of the field in Figure S1 in Supporting Information S1. Both Figures 2i and S1i in Supporting Information S1 show features **c** and **h** in regions of relatively weak magnetic field, whereas **e** and **g** appear to visually align with the strong field associated with the Northern Hemispheric Flux Band. The regions **a**, **b** and **f** are within ∼20° latitude of magnetic features but are not perfectly collocated.

Figure 2ii reveals that Jupiter possesses extremely localized regions of high dip angle across the planet, unlike the Earth where strongly inclined field lines are concentrated at high latitudes (Laundal et al., 2017; Schunk & Nagy, 2009). They also appear to approximately coincide with where the field is strongest (Figure 2i). Some of the ionospheric features align within ∼30° of near-perpendicular field lines (where field lines are close to vertical relative to the 1bar pressure level), including **a**, **e**, **g**, **h**, and **f**. Meanwhile, **b** and **c** are well contained within ∼30° of near-parallel field lines (where field lines are near-horizontal to the one bar pressure level). **d** is coincident with 0° dip angle and closely follows the B_r contour of 0G in Figure S1i in Supporting Information S1, indicating that it is likely to be an ionospheric signature of the horizontal field lines at Jupiter's magnetic equator. This suggests that the H_3^+ features may be magnetically bimodal, either associated with large or small dip angles.

Past measurements have shown that the broad-scale polar emission is dominated by high temperatures (O'Donoghue et al., 2021), and we estimate this temperature gradient extends to latitudes of ∼35°. Therefore, we restrict to latitudes between ±35° for both Figures 3 and 4, and display how the discrete H_3^+ emission features are lost if Figure 1's full extent is similarly analyzed in Figure S2 in Supporting Information S1.

Restricting to latitudes of ±35° effectively removes the effects of the auroral emissions across the map. However, the equatorward edge of the northern auroral emission "bleeds" into the non-auroral emission across 160–270°W, presumably due to the temperature gradient from the aurora to the equator. As a result, we mask the emission within the region affected by the auroral bleeding (160–270°W and 25–35°N) for both Figures 3 and 4. The inclusion of the masked region has minimal effects on the results, as shown by Figure S3 in Supporting Information S1, and it efficiently removes a bright feature (labeled **x**) which dominates the non-auroral emissions across 0–15G and ~25–65° dip angle.

Figure 3 shows how the H_3^+ brightness varies with (i) B_{Total}, (ii) absolute dip angle and (iii) both parameters simultaneously. Figure 3i displays a decreasing gradient in the H_3^+ brightness with increasing field strength, where the dimmest emissions occur at ~7G. Above this, the gradient in B_{Total} appears to have little effect on the ionospheric brightness. For Figure 3ii, the darkest emissions are concentrated at 0–15° and ~70–90°, which is consistent with the hypothesis of bimodal dip angle features. Similarly, there are clear brightness minima at 0–10° and 80–90° in Figure 3iii as a result of features **d** and **f** respectively. There is also a broad dimming across 30–65° and 7–16G, where the darkest emissions occur at 45–65° and 12–16G, and is presumably due to the coincidence of the bases of features **g** and **e** with the bottom of the Northern Hemispheric Flux Band. The relatively bright emissions about 45–70° and 6–8G are likely from the emissions equatorward and surrounding feature **f**.

For Figure 4, we split the constrained data into 45° longitude bands and calculate the median brightness for each band. We further bin the data into 5° dip angle bins and identify each dip angle bin where the H_3^+ emission is above (brighter than) or below (dimmer than) the median for a given longitude band. The northern and southern magnetic hemispheres correspond to where dip angles are positive and negative, respectively. We present a stacked histogram of the H_3^+ brightness relative to the median across all longitude bands, and show the percentage below the median, for each dip angle bin. Figure S4 in Supporting Information S1 represents an analogous plot to Figure 4, with the inclusion of the masked region between 160 and 270°W and 25–35°N.

T. S. Stallard et al. (2018) found that the Dark Ribbon **d** is relatively well-contained within ±5° of the JRM09 magnetic equator, and it is the one of the most prominent features across all longitudes in Figure 4, with 100% of the data below the median brightness within ±5° of the magnetic equator. Furthermore, **f** is also distinct as 100% of the H_3^+ emission is dimmer than the median between −75 and −90° dip angle across longitudes 45–135°. Notably, this is the only region where near-perpendicular field lines are observed in the southern magnetic hemisphere, just poleward of the Great Blue Spot. Figure 4 highlights the bimodality between equatorial H_3^+ emission and dip angle in the southern magnetic hemisphere. Significant dimming is associated with either near-parallel (0°) or near-perpendicular (−90°) field lines, with the strongest dimming occurring about the magnetic equator.

The northern magnetic hemisphere, where magnetic dip angles are positive, is less straightforward. We observe significant reductions from the median brightness for dip angles of +10–25° due to the combination of feature **b** and the diffuse darkening adjacent to **c** in Figure 1 (this darkening is also present across 35–50° dip angle), as well as +50–70° (the bases of both features **g** and **e**). This is perhaps indicative of a multi-modal distribution in the north, which may also explain the dimming across dip angles of 30–65° in Figure 3iii.

2.2. Magnetic Field Line Mapping

To firstly investigate the possibility of interhemispheric magnetic conjugacy as a potential source for the features, we traced magnetic field lines from the ionospheric features to their magnetically conjugate point in the opposing hemisphere (Figure 5). Figure 5 shows partial interhemispheric mapping between features **f** and **g**, where field lines from feature **f** map to **g**, but not all field lines from **g** map to **f**, with significant regions instead mapping to relatively bright regions surrounding **f**. We argue that they are magnetically linked to the high field anomalies in the opposing hemisphere, rather than to one another, potentially indicating a conjugate signature of these high flux regions. Since the remaining H_3^+ emission features do not trace to higher field strength locations in the opposing hemisphere, interhemispheric transport may not be the primary source for these localized variations in the Jovian ionosphere.

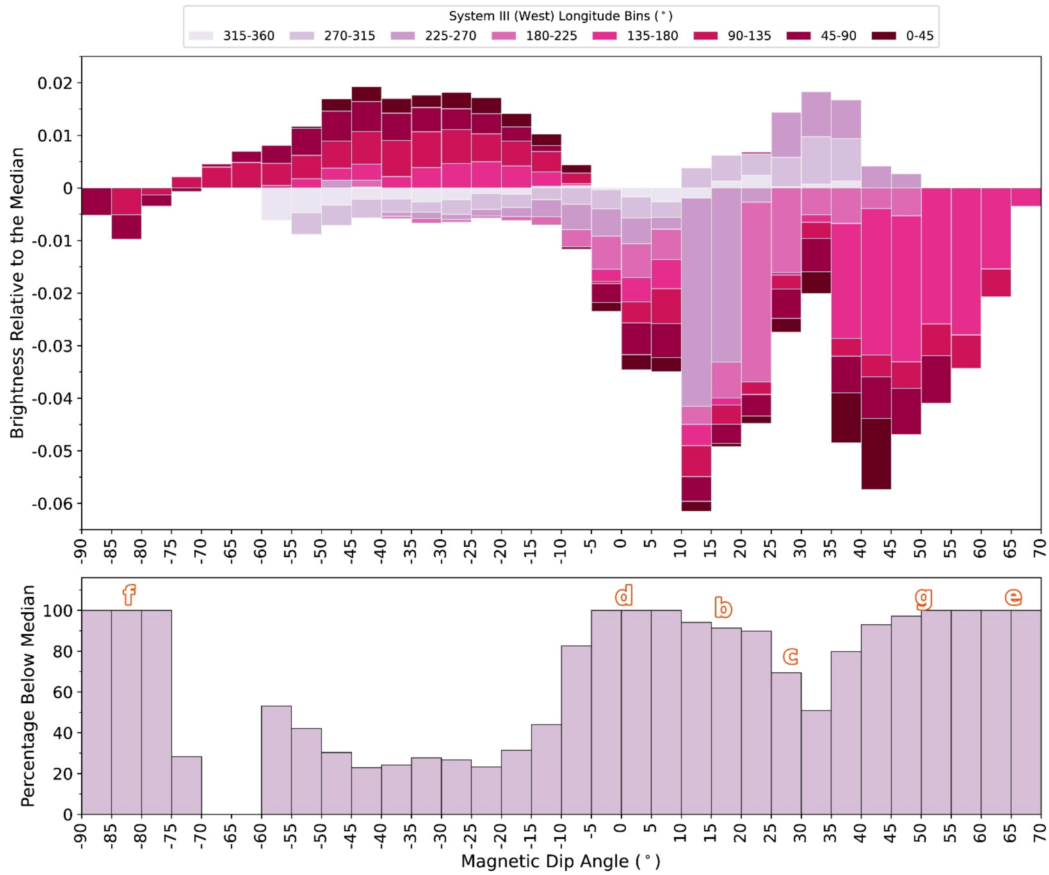

Figure 4. A stacked histogram displaying the distribution of the H_3^+ emission relative to the median brightness for various 45° longitude bins (indicated by colors) as a function of magnetic dip angle (°), and the percentage below the median for each 5° dip angle bin is also shown at the bottom. The area between 160 and 270°W and 25–35°N is masked from this figure.

To explore other potential sources, we traced field lines out to various M-shells, in steps of $0.05R_J$, 360° around the planet in 10° longitude intervals. The M-shell represents a given non-dipolar field line which intersects the equatorial plane at a radial distance equal to M. We plot the ionospheric magnetic footprint locations in Figure 6, and show that the H_3^+ features map to be within $4.00R_J$ in the Jovian magnetosphere.

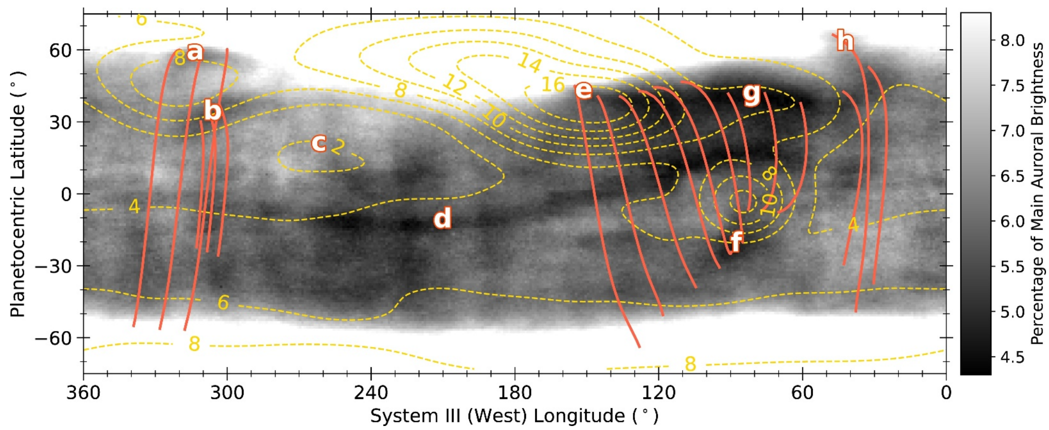

Figure 5. Magnetic field lines (orange-red) which originate from regions of depleted H_3^+ emissions are traced to their corresponding magnetic conjugate points in the opposing hemisphere. Contours of total magnetic field strength (G) have also been displayed (gold).

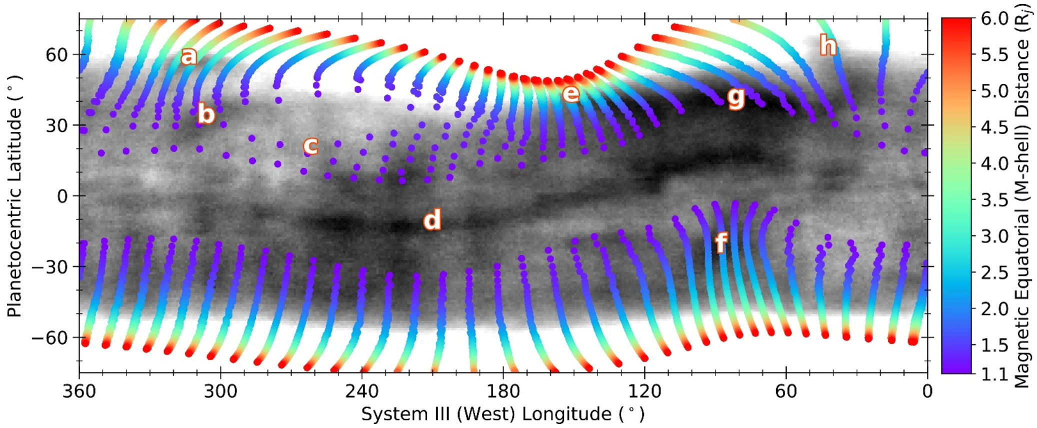

Figure 6. Ionospheric footprint locations for traced magnetic field lines, separated by 10° longitude, at various M-shell distances, in steps of $0.05R_J$.

2.3. Discussions on the Magnetic Shaping of the Ionosphere

We now interpret the various magnetic correlations presented in this analysis. Figures 2–4 show how large-scale irregularities in Jupiter's ionospheric emissions appear broadly associated with both low and high field strength, but this alone is not an accurate proxy.

Equatorial H_3^+ emission is dimmer at preferential dip angles, with one of the largest reductions occurring about the magnetic equator. In Figure 4, emission is strongly diminished either at dip angles of 0° or approaching 90° in the southern magnetic hemisphere. However, the opposing hemisphere possesses a more complicated distribution, with distinct departures from the median brightness at 0°, 10–25° and 50–70°, perhaps indicative of an additional effect governing the north. Figure S5 in Supporting Information S1 is an analogous plot to Figure 4 for B_{Total} and Figure S6 in Supporting Information S1 shows the effects of omitting the mask on the region including the auroral bleeding. The H_3^+ brightness does not deviate from the median as significantly, yet H_3^+ is consistently darker about 5G, ~7G, 8.5–12.5G and <13G in Figure S5 in Supporting Information S1. Given the distinct magnetic features across 90–135° longitude, we may consider the field strength to be the secondary effect in this region.

The significant asymmetry and variability in the field structure between conjugate hemispheres may drive different manifestations of the same magnetic disturbance. This could introduce local alterations in the upper atmospheric properties, suggesting that the ionosphere-magnetosphere coupling is unique across the entire planet (Laundal et al., 2017). Gradients in the Pedersen conductance can affect the altitude at which ions become coupled to the field, potentially resulting in the mixing of H_3^+ and electron layers, thus generating currents and inducing vertical transport either locally or between hemispheres.

We suggest that the likely driver for the dark H_3^+ emission features is localized reductions in the ion density within Jupiter's non-auroral ionosphere, as opposed to local decreases in temperature. Quasi-stable low temperature structures within the thermosphere would be difficult to maintain without constant driving in order to prevent them being smoothing out due to the thermal gradient between the auroral regions and mid-latitudes (Lam et al., 1997).

Above 600 km, H^+ ions dominate the Jovian ionosphere with their long chemical lifetime of ~1 Jovian day relative to ~1000 s for H_3^+ (Barrow et al., 2012). Under the assumption of photochemical equilibrium, where chemical timescales are relatively minor compared to timescales for transport, the density of H_3^+ is inversely proportional to the local electron density (L. Moore et al., 2004). There is reason to anticipate that Jupiter's ionosphere is not in full photochemical equilibrium (e.g., Mendillo et al., 2022), primarily because H^+ is the dominant species and is highly mobile. Yet it may be expected that isolated regions of reduced H_3^+ density are induced by a local enhancement in the H_3^+ chemical loss rate due to the presence of relatively high H^+ (and electron) densities.

We speculate that such conditions arise through vertical transport or via energetic particle precipitation from the inner Jovian magnetosphere, where the former is intrinsically entwined with the magnetic field geometry (L.

Moore et al., 2004). A reduction in the H_3^+ emission at high dip angles may indicate its vertical transport to lower/higher altitudes, thereby driving H_3^+ below the homopause where it is lost to proton transfer with methane, or up in altitude and causing a local minimum in the plasma density. Alternatively, it could imply precipitation into the equatorial ionosphere from the innermost magnetosphere, as observed by Juno (Kurth et al., 2025), or that high dip angles lead to a local minimum in the vertical transport induced by neutral winds, thus allowing a relatively large concentration of H^+ to build up. Low emission at low dip angles may suggest the electrodynamic transport of H_3^+, resulting in upward or downward drifting of plasma akin to at Earth (Laundal et al., 2017; Schunk & Nagy, 2009), or the inhibition of neutral wind driven ion motion. Both extremes are observed at Jupiter, resulting in the non-auroral H_3^+, produced by solar photoionization, which is strongly modulated by electrodynamic processes that are intimately linked with the local magnetic field structure.

Notably, the location of feature **g** coincides with a continuous enhanced neutral atmospheric emission known as the "H Ly-α bugle" (Melin & Stallard, 2016). Its production has been suggested to require either an increased population of H or elevated thermal velocities of the H ions. The latter creates wavelength-broadened Ly-α wings which increase the overall H Ly-α brightness, while the former involves an enhanced flux of soft electrons leading to electron recombination of H_3^+ that could be driven by a vertical $\mathbf{E} \times \mathbf{B}$ drift at the magnetic equator.

Recently, the James Webb Space Telescope observed the ionosphere above Jupiter's Great Red Spot (Early Release Science #1373, de Pater et al. (2022)) and revealed the instantaneous structure to be driven by transient gravity wave activity due to strong coupling to the lower atmosphere (Melin et al., 2024). No clear decrease in the H_3^+ density at the magnetic equator was found, but their spatial coverage was limited and they argued the need to temporally average over longer timescales to expose the electrodynamic molding of the ionosphere.

At Earth, the upward $\mathbf{E} \times \mathbf{B}$ force due to the horizontal field at the magnetic equator drives plasma up in altitude, leading to a local reduction with enhancements either side as the plasma gravitationally diffuses down the field lines, generating the Equatorial Ionization Anomaly (Schunk & Nagy, 2009). If such processes were to occur at Jupiter, its magnitude and direction would depend on the gradients in the ion and neutral ionospheric wind patterns, and since these are not well constrained at Jupiter, we can only speculate. Previous observations found indications of small-scale structure in the bulk H_3^+ flows, but these were inside of the derived errors (Johnson et al., 2016). Further modeling is needed to determine if this is occurring at Jupiter, especially given that the constituents of terrestrial plasma possess longer chemical lifetimes than that of H_3^+ (Miller et al., 2020; L. Moore et al., 2018; Schunk & Nagy, 2009), but that is beyond the scope of this study.

If there is ionosphere-magnetosphere coupling in these key regions, Figure 6 shows that the features magnetically map to be well within the volcanic moon Io's orbit ($5.9R_J$), and so we may eliminate field-aligned precipitation from the Io plasma torus as a possible driver. The inner magnetosphere ($<10R_J$) contains the primary source of plasma production, inner ring systems, radiation belts, innermost satellites, and Jupiter's magnetic field aids the trapping of ~1 GeV protons and >70 MeV electrons in this region (Roussos et al., 2022).

Charged particles propagating in the near Jupiter environment will orbit about a magnetic field line whilst radially drifting around the planet, with the direction of motion characterized by the particle's charge. If a magnetic field gradient is present, the azimuthal motion, along with the radial component of the magnetic field, results in a force acting against the particle's motion and in the direction of lower magnetic intensity. Its motion is slowed until it is forced to reverse its direction and is magnetically mirrored back along the field line, leading to a bounce motion between its northern and southern mirror points (Abel & Thorne, 2003). The strength of the mirror force varies as a function of the magnetic field strength, with a higher field strength producing a larger mirror force, and the field strength varies as a function of longitude. Longitudinal variations in the magnetic field strength can therefore scatter energetic charged particles such that they cannot be deflected sufficiently by the magnetic field intensity, and mirror at such low altitudes that they precipitate into the atmosphere (Abel & Thorne, 2003). Therefore, we may expect any H_3^+ brightness governed by particle precipitation to vary with magnetic field strength. The field across many of the features varies significantly, yet their brightness is relatively uniform (Figure 2i). As they appear to be quasi-stable over periods of years, any interactions with an external source would need to be long-lived and fixed in System III longitude, making it difficult to justify a variable external driver.

Nevertheless, for M-shells 1.10–1.35R_J, the field strength at the ionospheric footprints is at a minimum at **c**, whereas further away from the planet, we map to darkenings **f** and **h** (Figures 2i and 6). This change magnetically traces to a shift from a proton-rich to an electron-dominant population within Jupiter's inner radiation belts

(Roussos et al., 2022). If energetic particles are scattered into the non-auroral ionosphere, they could alter the local plasma conditions, current structure and subsequently the vertical mixing of H_3^+, and so may play a part in shaping some of the H_3^+ emission features.

Juno has directly sampled equatorial ionospheric populations using the Jovian Auroral Distributions Experiment Ion (JADE-I) sensor (Valek et al., 2019, 2020) and the Juno Waves instrument (Kurth et al., 2025). JADE-I has measured continuous signatures of heavier ions which vary in intensity, but do not change significantly with longitude, and are integrated with the lighter ions from the upper atmosphere (Valek et al., 2020). The authors hypothesized a magnetospheric origin, suggestive of coupling between the planet and inner magnetosphere, in agreement with this study. Furthermore, inferred ionospheric electron densities from the Waves instrument have shown distinct variations that appear to be somewhat organized to the Jovian magnetic field, as well as indications of mid-latitude particle precipitation into the atmosphere (Kurth et al., 2025), also harmonious with the findings of this work.

The re-analyzed 1995–2000 campaign represents the only observations to-date which provide a global view of the ionosphere with the sensitivity required to capture non-auroral variabilities (T. S. Stallard et al., 2018). Discrepancies with the magnetic measurements (Connerney et al., 2020, 2022) may be expected due the years separating the two independent data sets. Nonetheless, across the JRM09 and JRM33 epochs, the measured Jovimagnetic secular variation was localized to the Great Blue Spot (K. M. Moore et al., 2019; Simon et al., 2015), and the close alignment of **d** with the JRM33 equator suggests that Jupiter's magnetic equator has remained quasi-stable, which is a promising proxy. If the remaining H_3^+ features are akin to **d**, they may be broadly fixed in their System III longitudinal position for tens of years (T. S. Stallard et al., 2017), and so this direct comparison is compelling.

2.4. Summary and Conclusions

In this paper, we present a new analysis of ground-based observations of Jupiter's ionosphere with a direct comparison with magnetic field models from NASA's Juno mission. These results have revealed how Jupiter's magnetic field structure governs the long-term organization of its non-auroral upper atmosphere. Vertical transport of ionospheric H_3^+ ions may be present in specific locations, either locally generated or initiated by localized interactions with the surrounding plasma environment, and/or charged particle precipitation from the innermost magnetosphere may be occurring.

1. *The Great Cold Spot*. Coincident with a region of near-perpendicular magnetic field lines, highlighting one of the extremes of the bimodality between long-term ionospheric emissions and the geometry of the Jovian field.
2. *Northern Ionospheric Anomaly*. This feature remains unexplained.
3. *Broad region of enhancement*. A region of relatively weak field surrounded by complicated magnetic field geometry, and magnetically traces to a proton-rich environment within the inner radiation belts.
4. *Dark Ribbon*. Co-located with the parallel magnetic field lines about the magnetic equator, displaying the other extreme of the bimodal relationship between ionospheric emissions and the magnetic field's geometry.
5. *Head of the Northern Silhouette*. Located within the region of highest magnetic field strength (~17.85G) as well as near-perpendicular magnetic field lines. Both the extreme field strength and geometry may be affecting the structure of the ionosphere in this region.
6. *Southern Ionospheric Dark Spot*. Magnetically traces to the Northern Hemispheric Flux Band and is coincident with highly inclined magnetic field lines. This feature strongly highlights the bimodality present in the southern magnetic hemisphere, and traces to an electron-dominant population within Jupiter's inner radiation belts.
7. *Northern Silhouette*. Magnetically conjugate with the Great Blue Spot. The extreme magnetic field strength and geometry may also be playing a role in the low emission at this location.
8. *Tail of the Northern Silhouette*. Relatively weak magnetic field strength, and also traces to an electron-dominant population in the radiation belts.

We endeavor to motivate future investigations to observationally constrain the drivers of these ionospheric features, such as global observations similar to the T. S. Stallard et al. (2018) map which include spectroscopic H_3^+ temperature and column-density measurements (akin to Roberts et al. (2025)). We also highlight the need for new global circulation models which incorporate complex magnetic field topology to model the plasma transport within the Jovian ionosphere, as well as improved magnetic mapping at low M-shells. Both previous and current studies are limited by their ability to sense the detail of this highly complex region, which challenges our current understanding and differs significantly from the auroral regions.

This study illustrates how ground-based observations can potentially track extremities in the planetary magnetic field, supporting Juno's extended mission as well as after its culmination, and how possibly the same can be achieved at other worlds in the absence of in-situ spacecraft. Since Jupiter is not alone in possessing a complex magnetic field, it is not unlikely that these ionospheric shadows occur at other giant planets, within our Solar System and further afar.

Data Availability Statement

The T. S. Stallard et al. (2018) data set used in this study is publicly available at https://doi.org/10.7910/DVN/KVQWNJ (T. Stallard, 2018). The data which supports the JRM33 magnetic field model is archived using the NASA Planetary Data System at https://doi.org/10.17189/1519711 and can be found at https://pds-ppi.igpp.ucla.edu/collection/JNO-J-3-FGM-CAL-V1.0 (Connerney, 2017). The data set supporting the Con2020 current sheet model can also be found at the NASA Planetary Data System https://pds-ppi.igpp.ucla.edu/search/default.jsp#. The open-source python package, JupiterMag, used to utilize both the JRM33 and Con2020 models can be found at https://github.com/mattkjames7/JupiterMag.git (where the corresponding journal can be found at https://doi.org/10.1007/s11214-023-00961-3).

Acknowledgments
K.L.K was supported by a Northumbria University Research Studentship at Northumbria University, UK. J.O. was supported by the STFC Ernest Rutherford Fellowship (ST/X003426/1) at the University of Reading, UK. L.M. and O. A. were both supported by Grant 80NSSC23K0661 issued through the NASA New Frontiers Data Analysis Program. H.M. was supported by the STFC James Webb Fellowship (ST/W001527/2) at Northumbria University, UK. I.J.R was supported in part by NERC grant NE/W003198/1 and STFC Grant ST/X001008/1. K.R was supported by NASA FINESST Grant 80NSSC23K1637. P.I.T. was funded by UK Science and Technology Facilities Council (STFC) Studentship ST/X508548/2. This research was supported by the International Space Science Institute (ISSI) in Bern, through ISSI International Team Project 23-592 (Jupiter's non-auroral ionosphere). The authors would like to acknowledge invaluable technical support provided by Alexander D Tempest at Northumbria University, UK.

References

Abel, B., & Thorne, R. M. (2003). Relativistic charged particle precipitation into Jupiter's sub-auroral atmosphere. *Icarus*, *166*(2), 311–319. https://doi.org/10.1016/j.icarus.2003.08.017

Barrow, D., Matcheva, K. I., & Drossart, P. (2012). Prospects for observing atmospheric gravity waves in Jupiter's thermosphere using H3+ emission. *Icarus*, *219*(1), 77–85. https://doi.org/10.1016/j.icarus.2012.02.007

Bloxham, J., Moore, K. M., Kulowski, L., Cao, H., Yadav, R. K., Stevenson, D. J., et al. (2022). Differential rotation in Jupiter's interior revealed by simultaneous inversion for the magnetic field and zonal flux velocity. *Journal of Geophysical Research: Planets*, *127*(5), e2021JE007138. https://doi.org/10.1002/2014GL060814

Connerney, J. E. P. (2017). Juno fluxgate magnetometer calibrated data V1.0 [Dataset]. *NASA Planetary Data System*. https://doi.org/10.17189/1519711

Connerney, J. E. P., Kotsiaros, S., Oliverson, R. J., Espley, J. R., Joergensen, J. L., Joergensen, P. S., et al. (2018). A new model of Jupiter's magnetic field from Juno's first nine orbits. *Geophysical Research Letters*, *45*(6), 2590–2596. https://doi.org/10.1002/2018gl077312

Connerney, J. E. P., & Satoh, T. (2000). The H3+ ion: A remote diagnostic of the Jovian magnetosphere. *Philosophical Transactions of the Royal Society of London. Series A: Mathematical, Physical and Engineering Sciences*, *358*(1774), 2471–2483.

Connerney, J. E. P., Timmins, S., Herceg, M., & Jørgensen, J. L. (2020). A Jovian magnetodisc model for the Juno era. *Journal of Geophysical Research: Space Physics*, *125*(10), e2020JA028138. https://doi.org/10.1029/2020ja028138

Connerney, J. E. P., Timmins, S., Oliverson, R. J., Espley, J. R., Joergensen, J. L., Kotsiaros, S., et al. (2022). A new model of Jupiter's magnetic field at the completion of Juno's prime mission. *Journal of Geophsyical Research: Space Physics*, *127*(2), e2021JE007055. https://doi.org/10.1029/2021je007055

de Pater, I., Fouchet, T., Wong, M., Fry, P., Fletcher, L., Hueso, R., et al. (2022). JWST observations of the Jovian system from commissioning and ERS data. *AAS/Division for Planetary Sciences Meeting Abstracts*, *54*(306.07).

Drossart, P. (2019). H3+ as an ionospheric sounder of Jupiter and giant planets: An observational perspective. *Philosophical Transactions of the Royal Society*, *A377*(2154), 20180404. https://doi.org/10.1098/rsta.2018.0404

Drossart, P., Maillard, J., Caldwell, J., Kim, S. J., Watson, J. K. G., Majewski, W. A., et al. (1989). Detection of H3+ on Jupiter. *Nature*, *340*(6234), 539–541. https://doi.org/10.1038/340539a0

Gastine, T., Wicht, J., Duarte, L. D. V., Heimpel, M., & Becker, A. (2014). Explaining Jupiter's magnetic field and equatorial jet dynamics. *Geophysical Research Letters*, *41*, 5410–5419. https://doi.org/10.1002/2014GL060814

Geballe, T. R., Jagond, M. F., & Oka, T. (1993). Detection of H3+ infrared emission lines in Saturn. *The Astrophysical Journal Letters*, *408*, 109–112.

James, M. K., Wilson, R. J., Vogt, M. F., Provan, G., Karman, A., Brennan, M. J., & Cowley, S. W. H. (2022). JupiterMag (v1.3.1). https://doi.org/10.5281/zenodo.10602418

Johnson, R. E., Melin, H., Stallard, T. S., Tao, C., Nichols, J. D., & Chowdhury, M. N. (2018). Mapping H3+ temperatures in Jupiter's northern auroral ionosphere using VLT-CRIRES. *Journal of Geophysical Research: Space Physics*, *123*(7), 5990–6008. https://doi.org/10.1029/2018ja025511

Johnson, R. E., Stallard, T. S., Melin, H., Miller, S., & Nichols, J. D. (2016). Measurements of the rotation rate of the Jovian mid-to-low latitude ionosphere. *Icarus*, *280*, 249–254. https://doi.org/10.1016/j.icarus.2016.06.026

Kurth, W. S., Faden, J. B., Waite, J. H., Sulaiman, A. H., Elliott, S. S., Hospodarsky, G. B., et al. (2025). Electron densities in Jupiter's upper Ionosphere inferred from Juno Plasma wave observations. *Journal of Geophysical Research: Planets*, *130*(3), e2024JE008845. https://doi.org/10.1029/2024je008845

Lam, H. A., Achilleos, N., Miller, S., Tennyson, J., Trafton, L. M., Geballe, T. R., & Ballester, G. E. (1997). Baseline spectroscopic study of the infrared auroras of Jupiter. *Icarus*, *127*(2), 379–393. https://doi.org/10.1006/icar.1997.5698

Laundal, K. N., Cnossen, I., Milan, S. E., Haaland, S. E., Coxon, J., Pedatella, N. M., et al. (2017). North-south asymmetries in Earth's magnetic field. *Space Science Reviews*, *206*(1–4), 225–257. https://doi.org/10.1007/s11214-016-0273-0

Melin, H., Miller, S., Stallard, T., & Grodent, D. (2005). Non-LTE effects on H3+ emission in the Jovian upper atmosphere. *Icarus*, *178*(1), 97–103. https://doi.org/10.1016/j.icarus.2005.04.016

Melin, H., O'Donoghue, J., Moore, L., Stallard, T. S., Fletcher, L. N., Roman, M. T., et al. (2024). Ionospheric irregularities at Jupiter observed by JWST. *Nature Astronomy*, *8*, 1000–1007. https://doi.org/10.1038/s41550-024-02305-9

Melin, H., & Stallard, T. S. (2016). Jupiter's hydrogen bulge: A Cassini perspective. *Icarus*, *278*, 238–247. https://doi.org/10.1016/j.icarus.2016.06.023

Mendillo, M., Narvaez, C., Moore, L., & Withers, P. (2022). Jupiter's enigmatic ionosphere: Electron density profiles from the pioneer, Voyager, and Galileo radio occultation experiments. *Journal of Geophysical Research: Space Physics*, *127*(3), e2021JE007169. https://doi.org/10.1029/2021je007169

Miller, S., Stallard, T., Tennyson, J., & Melin, H. (2013). Cooling by H3+ emission. *Journal of Physical Chemistry A*, *117*(39), 9770–9777.

Miller, S., Tennyson, J., Geballe, T. R., & Stallard, T. (2020). Thirty years of H3+ astronomy. *Reviews of Modern Physics*, *92*(3), 035003.

Moore, K. M., Bloxham, J., Connerney, J. E. P., Jørgensen, J. L., & Merayo, J. M. G. (2017). The analysis of initial Juno magnetometer data using a sparse magnetic field representation. *Geophysical Research Letters*, *44*(10), 4687–4693. https://doi.org/10.1002/2017gl073133

Moore, K. M., Cao, H., Bloxham, J., Stevenson, D. J., Connerney, J. E. P., & Bolton, S. J. (2019). Time variation of Jupiter's internal magnetic field consistent with zonal wind advection. *Nature Astronomy*, *3*(8), 730–735. https://doi.org/10.1038/s41550-019-0772-5

Moore, L., Galand, M., Kliore, A. J., Nagy, A. F., & O'Donoghue, J. (2018). *Saturn's ionosphere, Saturn in the 21st Century*. Cambridge University Press, 196–223.

Moore, L., Mendillo, M., Müller-Wodarg, I. C. F., & Murr, D. L. (2004). Modeling of global variations and ring shadowing in Saturn's ionosphere. *Icarus*, *172*(2), 503–520. https://doi.org/10.1016/j.icarus.2004.07.007

O'Donoghue, J., Moore, L., Bhakyapaibul, T., Melin, H., Stallard, T., Connerney, J. E. P., & Tao, C. (2021). Global upper-atmospheric heating on Jupiter by the polar aurorae. *Nature*, *596*(7870), 54–57. https://doi.org/10.1038/s41586-021-03706-w

Rego, D., Miller, S., & Achilleos, N. (2000). Latitudinal profiles of the Jovian IR emissions of H+3 at 4 μm with the NASA infrared telescope facility: Energy inputs and thermal balance. *Icarus*, *147*(2), 366–385. https://doi.org/10.1006/icar.2000.6444

Rishbeth, H., & Garriott, O. K. (1969). *Introduction to ionospheric physics*. Academic Press.

Roberts, K., Moore, L., O'Donoghue, J., Melin, H., Stallard, T., Knowles, K. L., et al. (2025). Spatiotemporal variations of temperature in Jupiter's upper atmosphere. *Planetary Science Journal*, *6*(4), 92.

Roussos, E., Allanson, O., Nicolas, A., Bertucci, B., Branduardi-Raymont, G., Clark, G., et al. (2022). The in-situ exploration of Jupiter's radiation belts. *Experimental Astronomy*, *54*(2–3), 745–789. https://doi.org/10.1007/s10686-021-09801-0

Schunk, R. W., & Nagy, A. F. (2009). *Ionospheres: Physics, plasma physics, and chemistry* (2nd ed.). Cambridge University Press.

Simon, A. A., Wong, M. H., & Orton, G. S. (2015). First results from the Hubble OPAL Program: Jupiter in 2015. *The Astrophysics Journal*, *812*(55), 55. https://doi.org/10.1088/0004-637x/812/1/55

Stallard, T. (2018). The magnetospheres of the outer planets infrared data archive: IRTF NSFCAM 1995-2000. *Harvard Dataverse*. https://doi.org/10.7910/DVN/KVQWNJ

Stallard, T., Miller, S., Millward, G., & Joseph, R. D. (2002). On the dynamics of the Jovian ionosphere and thermosphere: II. The measurement of H3+ vibrational temperature, column density, and total emission. *Icarus*, *156*(2), 498–514. https://doi.org/10.1006/icar.2001.6793

Stallard, T. S., Burrell, A. G., Melin, H., Fletcher, L. N., Miller, S., Moore, L., et al. (2018). Identification of Jupiter's magnetic equator through H3+ ionospheric emission. *Nature Astronomy*, *2*(10), 773–777. https://doi.org/10.1038/s41550-018-0523-z

Stallard, T. S., Melin, H., Miller, S., Moore, L., O'Donoghue, J., Connerney, J. E. P., et al. (2017). The great cold spot in Jupiter's upper atmosphere. *Geophysical Research Letters*, *44*(7), 3000–3008. https://doi.org/10.1002/2016gl071956

Stallard, T. S., Melin, H., Miller, S., O'Donoghue, J., Cowley, S. W. H., Badman, S. V., et al. (2012). Temperature changes and energy inputs in giant planet atmospheres: What we are learning from H3+. *Philosophical Transactions of the Royal Society A*, *370*(1978), 5213–5224. https://doi.org/10.1098/rsta.2012.0028

Trafton, L. M., Geballe, T. R., Miller, S., Tennyson, J., & Ballester, G. E. (1993). Detection of H3+ from Uranus. *The Astrophysical Journal*, *405*, 761–766. https://doi.org/10.1086/172404

Valek, P. W., Allegrini, F., Bagenal, F., Bolton, S. J., Connerney, J. E. P., Ebert, R. W., et al. (2019). Jovian high-latitude ionospheric ions: Juno in situ observations. *Geophysical Research Letters*, *46*(15), 8663–8670. https://doi.org/10.1029/2019gl084146

Valek, P. W., Bagenal, F., Ebert, R. W., Allegrini, F., McComas, D. J., Szalay, J. R., et al. (2020). Juno in situ observations above the Jovian equatorial ionosphere. *Geophysical Research Letters*, *47*(12), e2020GL087623. https://doi.org/10.1029/2020gl087623

Wilson, R. J., Vogt, M. F., Provan, G., Kamran, A., James, M. K., Brennan, M., & Cowley, S. W. H. (2023). Internal and external Jovian magnetic fields: Community code to serve the magnetospheres of the outer planets community. *Space Science Reviews*, *219*(15), 15. https://doi.org/10.1007/s11214-023-00961-3